Title

Three-dimensional MRI-based statistical shape model and application to a cohort of knees with acute ACL injury

Journal

Osteoarthritis and Cartilage, 23(10)

ISSN

1063-4584

Authors

Pedoia, V

Lansdown, DA

Zaid, M

et al.

Publication Date

2015-10-01

DOI

10.1016/j.joca.2015.05.027

Peer reviewed

HHS Public Access

Author manuscript

Osteoarthritis Cartilage. Author manuscript; available in PMC 2016 October 01.

Published in final edited form as:

Osteoarthritis Cartilage. 2015 October ; 23(10): 1695–1703. doi:10.1016/j.joca.2015.05.027.

Three-Dimensional MRI-Based Statistical Shape Model and Application to a Cohort of Knees with Acute ACL Injury

Valentina Pedoia, Ph. D.[1], **Drew A. Lansdown, M. D.**[2], **Musa Zaid, B.S.**[1], **Charles E. McCulloch, Ph.D.**[3], **Richard Souza, P. T., Ph.D.**[2], **C. Benjamin Ma, M. D.**[2], and **Xiaojuan Li, Ph. D.**[1]

Drew A. Lansdown: LansdownDA@orthosurg.ucsf.edu; Musa Zaid: musa.zaid@ucsf.edu; Charles E. McCulloch: CMcCulloch@psf.ucsf.edu; Richard Souza: richard.souza@ucsf.edu; C. Benjamin Ma: MaBen@orthosurg.ucsf.edu; Xiaojuan Li: xiaojuan.li@ucsf.edu

[1]Department of Radiology and Biomedical Imaging, University of California, San Francisco

[2]Department of Orthopaedic Surgery, University of California, San Francisco

[3]Department of Epidemiology & Biostatistics, University of California, San Francisco

Abstract

Objective—The aim of this study is to develop a novel 3D magnetic resonance imaging (MRI)-based Statistical Shape Modeling (SSM) and apply it in knee MRIs in order to extract and compare relevant shapes of the tibia and femur in patients with and without acute ACL injuries.

Methods—Bilateral MR images were acquired and analyzed for 50 patients with acute ACL injuries and for 19 control subjects. A shape model was extracted for the tibia and femur using an SSM algorithm based on a set of matched landmarks that are computed in a fully automatic manner.

Results—Shape differences were detected between the knees in the ACL-injury group and control group, suggesting a common shape feature that may predispose these knees to injury.

Corresponding Author: Valentina Pedoia, PhD, Address: 185 Berry Street, Lobby 6, Suite 350 94107 San Francisco California; Tel: 415-5496136, Fax: 415-353-9425, valentina.pedoia@ucsf.edu.

Contributions:

- Conception and design: Xiaojuan Li,
- Algorithm Development: Valentina Pedoia,
- Analysis and interpretation of the data: Valentina Pedoia, Drew A. Lansdown, Musa Zaid
- Drafting of the article: Valentina Pedoia, Drew A. Lansdown, Xioajuan Li,
- Physical and Clinical interpretation of the results: Drew A. Lansdown, Richard Souza, C. Benjamin Ma,
- Statistical Expertise: Charles M. McCulloch
- Obtaining of funding: Xiaojuan Li, C. Benjamin Ma
- Review and proof of the manuscript: all authors.

Conflict of Interest: The authors have no conflicts of interests to disclose.

Some of the detected shape features that discriminate between injured and control knees are related to intercondylar width and posterior tibia slope, features that have been suggested in previous studies as ACL morphological risk factors. However, shape modeling has the great potential to quantify these characteristics with a comprehensive description of the surfaces describing complex 3D deformation that cannot be represented with simple geometric indexes.

Conclusions—3D MRI-based bone shape quantification has the ability to identify specific anatomic risk factors for ACL injury. A better understanding of the role in bony shape on ligamentous injuries could help in the identification of subjects with an increased risk for an ACL tear and to develop targeted prevention strategies, including education and training.

Keywords

Statistical Shape Modeling; Magnetic Resonance Imaging; Anterior Cruciate Ligament; Osteoarthritis

Introduction

Anterior cruciate ligament (ACL) injuries are one of the most common ligament injuries of the knee joint. Annual incidence is reported to be at least 81 per 100,000 in an age range between 10 and 64 years [1]. Identification of risk factors for ACL injury is an important step in the development of injury prevention strategies [2,3]. It is well known that the geometry of the tibiofemoral joint has a key role in controlling transmission of the large compressive and shear intersegmental forces across the knee. Therefore, in the last years there has been a great deal of focus on anatomic risk factors for ACL injuries [4,5,6,7].

Statistical Shape Modeling (SSM) is a promising mathematical tool that has the ability to characterize complex shapes in a brief but comprehensive feature vector using Principal Component Analysis (PCA) to reduce the dimensionality of the data [8]. SSM has the capability to analyze shape differences without *a priori* assumptions, instead identifying the features empirically.

SSM has been widely used with 2D radiographs for bone shape characterization. Gregory et al.[9] was the first to use SSM to study the association of the shape of the proximal femur with the occurrence of femoral neck fractures. This study clearly outlined how multiple geometric measurements are highly correlated and that a comprehensive approach to modeling and measuring the shape can be more effective. A similar strategy was then used by Lynch et al. [10] and Baker-LePain et al.[11] in studies aimed at exploring the role of hip shape in radiographic OA. Haverkamp et al.[12] determined aspects of bone shape in the knee that related to OA in a population-based cohort of 609 women.

Despite the widespread use of SSM with plain radiographs, the application in magnetic resonance imaging (MRI) is still a medical imaging challenge. However, the potential of SSM, coupled with the three-dimensional nature of MR imaging, has generated significant recent interest in the application to knee osteoarthritis[13,14]. Bredbenner et al. [13] demonstrated that variability in knee subchondral bone surface geometry will differentiate between patients at risk and those not at risk for developing OA using 3D SSM on a subset

of clinical knee MRI data from the Osteoarthritis Initiative (OAI) database. Recently, a study to examine whether 3D bone shape predicts the onset of radiographic knee osteoarthritis (OA) combining Active Appearance Model (AAM) and Linear Discriminant Analysis (LDA) was also presented[14].

Manual or semi-automatic techniques for the SSM extraction have produced good results in the 2D application but hardly applicable in 3D with acceptable results. This is one of the main reasons why there have been few MRI applications to date. The crucial step in the extraction of SSM is landmark matching. Several approaches have been proposed in the literature. Some of these are limited by the application of rigid transformation[15], while others use a non-rigid registration with iterative distortion[16,17] or features control points[18,19]. Others use an explicit representation of surface parameterization to minimize the length of the model [20,21]. Recently, Lombaert et al.[22] presented a matching strategy based on a vertex-to-vertex correspondence algorithm that implies the direct matching in a feature space regularized by using the spectral coordinates (FOCUSR). The technique showed powerful results in the brain surface matching but has not previously been applied to knee MRI data nor used to extract a SSM.

The goal of the present study is twofold: 1) to develop a new method for the automatic 3D SSM extraction based on FOCUSR; and 2) to apply this method in knee MRIs in order to extract and compare relevant shapes of the tibia and femur in patients with and without acute ACL injuries. The present study design does not allow for defining shape features that can predict the injury, but it can clarify the relationship between bony anatomy and ligamentous injury and it can help in formulating specific hypotheses for future investigations.

We hypothesize that there are specific bone shape differences between the ACL injured knees and control knees and between the contralateral and control knees.

Methods

Subjects

Bilateral knees were scanned using a 3 Tesla MRI scanner (GE Healthcare, Milwaukee, WI, USA) with an 8-channel phased array knee coil (Invivo, Orlando, FL, USA) for 50 patients with complete ACL injuries prior to surgical reconstruction within 1-26 weeks after injury (mean = 7.63 ± 4.52 weeks, median = 6.42) (age = 29.6± 8.2 years, BMI = 24.1± 2.8 Kg/m^2, 21 female). Nineteen control subjects (age = 31.1 ± 4.4 years, BMI = 24.6 ± 2.2 Kg/m^2, 7 female) with no history of knee injuries and osteoarthritis underwent unilateral knee MR imaging at a baseline point. Five healthy volunteers were scanned twice, with repositioning between scans, to assess the reliability of the overall strategy for the automatic 3D SSM extraction. Three of these subjects were also segmented twice by different users, each with an experience of more than 30 knees segmented with this protocol.

Imaging Protocol

The imaging protocol included sagittal T2 fast spin-echo (FSE) images with TR/TE = 4000/49.3ms, slice thickness of 1.5 mm, spacing of 1.5 mm, field of view of 16 cm, 512 × 512 matrix size and echo train length 9.

Image Post Processing

Image processing was performed using an in-house Matlab-based program. The tibia and femur were segmented semi-automatically using a strategy based on edge detection that considers a three-dimensional smoothness constraint[23]. The algorithm generates an estimation of the border that is then manually adjusted to fit the cortical border of tibia and femur. Bezier spline interpolation was used to obtain a dense cloud of points. This technique was previously applied on the same MRI sequence for the bone segmentation showing excellent reproducibility in the computation of knee kinematic parameters such as anterior tibia translation and internal tibia rotation [24].

A three-dimensional triangulated mesh of the bone was extracted using the Marching Cube algorithm, and a Laplacian smoothing was applied to the mesh[25, 26].

The analysis was conducted individually for the tibia and femur to be invariant to the relative position of the joint. Moreover, all the surfaces of the tibia and femur were rigidly registered with Iterative Closest Point matching, so only distinct shape features remained in the SSM. An iterative process was employed to define the best reference knee in the dataset using the sum of the registration errors as a metric to evaluate each candidate surface.

All the vertices of the reference were mapped on all the surfaces in the dataset using a fully automatic landmark-matching algorithm. The strategy used in this study was based on the one recently proposed by Lombaert et al. [22]. The maximum and minimum local curvatures were used for coupling, homologous points on two surfaces (Figure 1). Both these features were locally defined on the surfaces and used to identify the landmark matching solved using Coherent Point Drift[27]

A total of 8,120 and 11,222 landmarks are identified for the tibia and the femur, respectively. Each surface in the dataset x_i is described by a set of 3D coordinates, corresponding with the position of the landmarks on the surface. Each surface can be considered as a point in a $3*L$ dimension space where L is the total number of landmarks. The mean surface can be computed as:

$$\overline{x}=\frac{1}{N}\sum_{i=1}^{N}x_i \quad (2)$$

where N is the number of surfaces in the dataset and x_i is the vector of the landmark coordinates of each subject. The covariance matrix S was used in order to calculate the variation of shapes from the mean shape:

$$S=\frac{1}{N-1}\sum_{i=1}^{N}(x_i-\overline{x})(x_i-\overline{x})^T \quad (3)$$

Eigen vector decomposition is then computed on the covariance matrix to extract the most important modes of variation of all the surfaces from the mean surface (Principal Component Analysis, PCA).

Physical Interpretation of the Model

PCA provides an orthonormal basis; therefore each mode describes a different aspect of the bone shape uncorrelated with the others. The effect of each mode can be modeled individually by generating new 3D surfaces that are different from the average surface just for the specific shape feature described by the modeled mode.

The physical representation of the modes was investigated by changing the value of each mode from the mean, to the mean ± 3 standard deviations (SD) and observing the displacement of the landmarks from the average surface using three-dimensional colored meshes.

The color of each face of the mesh is related to the local Euclidean distance (mm) between the position of the closest landmark in the average surface and in the modeled surface.

The 3 components of the Euclidean distance in the: posterior to anterior, medial to lateral and distal to proximal directions are computed and 3 colored mesh are created for the visualization of the results.

The distance is displayed as positive (red) if the local displacement is towards the anterior, lateral, and proximal for tibia and distal for femur directions; and the distance is displayed as negative (blue) if the displacement is towards the posterior, medial, and distal for tibia and proximal for femur directions.

Statistical Analysis

The reliability of the method was assessed by calculating the Root Mean Square Coefficient of Variation for each modal value in the 5 subjects scanned and re-scanned after repositioning; and in 3 of these 5 subjects after re-processing by different user. The inter-user segmentation reliability is also computed in terms of mean surface distance.

A bootstrap analysis was performed to assess the robustness of the SSM using five bootstrap replications and rebuilding the SSM each time. A resampling with replacement was done for 70% of the surfaces in the original dataset and the model was computed and evaluated in comparison with the one obtained with the fully sampled dataset. The stability of the PCA basis was evaluated qualitatively by observing the colored mesh obtained according to the vertex Euclidean distance between the mean surface and the surfaces obtained changing the values of the first 5 modes. Moreover, the 3 surfaces modeled from each bootstrap replication in each mode (mean ± 3 SD) were compared to the surfaces obtained from the original model. The mean of the distances of all the vertexes was computed as a similarity matrix for each bootstrap experiment using the following equation:

$$D_{i,j}=\frac{1}{L}\sum_{k=1}^{L}|l_{i,j,k}-l_{i_o,j,k}| \quad (4)$$

where $D_{i,j}$ is the mean distance computed for i_{th} bootstrap experiment and j_{th} mode, L is the total number of landmarks that define the surface, $l_{i,j,k}$ is the k_{th} 3D coordinate vector of the surface obtained modeling the j_{th} mode in the i_{th} bootstrap, and $l_{i,j,k}$ is the k_{th} 3D coordinate vector of the surface obtained modeling the j_{th} mode in the original model

A second set of analyses was performed to evaluate the association between the bone shape and ACL injury. An unpaired T-test was used to evaluate the differences between injured and control knees and between contralateral and control knees. A paired T-test was used for the evaluation of statistical differences between injured and contralateral knees. A Bonferroni correction was applied to account for multiple comparisons due to the analysis of the different modes.

There is no clear agreement among users of PCA on how to incorporate scale. Due to correlation of size with other shape features, this information could not be completely encapsulated just in one mode. To avoid any misinterpretation of these data the evaluation of the groups' difference was performed also after the Euclidean alignment of the surfaces, which removes any effect of the size. In the following, the 2 models are called “scale-preserved” and “Euclidean”. Reliability, robustness and physical interpretation are reported here using the scale-preserved model.

The significant modes of the scale-preserved model were then used in a Generalized Linear Model (GLM) to assess the ACL injured/control and contralateral/control classification performance of the identified model, A 75%-25% K-fold cross validation was used to test the performances, and the ROC area under the curve used as evaluation metric. Gender differences were also tested through unpaired T-test.

Results

Model Reliability

The average surface distances for the 3 cases segmented twice are 0.75 mm, 0.69 mm, and 0.92 mm for the femur and 0.76, 0.63 mm, and 0.96 mm for the tibia.

Table 1 shows the inter user RMS-CVs computed for the 3 volunteers evaluated for the first ten modes of both femur and tibia. The average RMS-CV is equal to 7.23% and 7.27% on the first 10 modes and 2.65% and 4.89% in the first 5 for femur and tibia respectively.

Table 1 is also shows the scan/re-scan RMS-CVs for all the 5 volunteers computed for the first ten modes of both femur and tibia. The average RMS-CV is equal to 12.25% and 14.7% on the first 10 modes and 7.33% and 12.25% in the first 5 for femur and tibia respectively.

Model Robustness

Figure 2 and Figure 3 show the results obtained in the bootstrap experiment for femur and tibia, respectively. The mean of the distances of all vertices is included in the figure as well.

The results obtained show good stability of the model for the femur in the first four modes, showing similar vertex displacement distribution, and the average distance between points is always less than 2 mm. In mode 5, the first, second, and last bootstraps show some notable differences in the reconstructed femur suggesting a mode order switching.

Slightly higher instability is observed in the tibia's model, with mode 1 and mode 3 showing completely stable behavior along the five bootstrap experiments.

Association between bone shape and ACL injury

Figure 4 shows the PCA normalized accumulated variation for all the modes of the model both for femur and tibia. This representation describes the compactness of the model.

In the first 10 modes of tibia and femur is represented 85.1% and 84.8% of the entire variability of which 78.5% and 77.2% in the first 5 modes.

Due to the results obtained in the reliability and robustness experiments, the first 5 modes are tested to study the association between bone shape and ACL injury. The compactness of the model allows us to describe a large percentage of the entire variability of the dataset with a small number of modes.

Table 2 summarizes the main results obtained with scale-preserved and Euclidean models The 2nd mode of the femur (F2) was observed to be significantly different between injured and control group showing an increase of 12% in average from control to injured (the average scan/rescan reliability for this mode is 7.23%). The differences of the same modes between contralateral and control group were not statistical significant if the Bonferroni correction is considered. There were not statistically significant differences between injured and contralateral groups in the paired T-test. The 3rd mode of the tibia (T3) was observed to be significantly different between injured and control groups and between contralateral and control groups, showing an increase of 29% in average from control to injured (the average scan/rescan reliability for this mode is 8.27%). There were not statistically significant differences between injured and contralateral group in the paired T-test. Consistent results are obtained with the model obtained after removing the scale affect. The ranking of the significant modes is different but the physical meaning is preserved F2 and T3 in the scale-preserved model represent the same shape features described in F1 and T2 in the Euclidean model.

A GLM model was developed with F2 and T3 of the scale-preserved model and used to assess the ACL vs. control and contralateral vs control classification performances. The mean AUCs obtained in the 69 K-fold experiment was 0.75 (95 % C.I. 0.62-0.86) in the classification of injured vs control and 0.70 (95 % C.I. 0.57-0.83) in the classification of contralateral vs control. Significant differences were found between genders in the first modes for both tibia and femur ($p<0.001$) and F2 ($p = 0.01$) of the scale-preserved model.

Physical Interpretation of the Scale-Preserved Model

For the femur, the first mode is related to the size, the second related to the relative distance between the condyles, and the third related to the condylar width and height, with the effect observed more in the lateral side than medial. Significant differences between injured and control femurs were found in F2. The ACL injured subjects showed narrower intercondylar notch than controls.

For the tibia, the first mode is related to size, the second to the medial posterior curvature of the tibial plateau, and the third to elevation of the anteromedial tibial plateau. Significant differences between injured and control tibia were found in T3. The ACL injured subjects showed an elevation in the anteromedial tibial plateau. Figure 5 shows the effect of changing modes F2 and T3. The first row shows deformations related to mean + 3SD and the second row deformation related to mean -3SD.

Figure 6a shows the displacement of the vertices of the second mode of femur in the posterior-anterior, medial-lateral and superior-inferior directions obtained after modeling the difference between the average control and average ACL injured femurs. The medial-lateral direction, which corresponds to the notch in 2D images, is the most involved in the deformation showing a maximum displacement equal to 1.6 mm. Moreover, a movement of the side vertices in superior-inferior direction can be noted with a comparable magnitude (maximum displacement 1.11 mm). A small increase in size of the femoral trochlear surface area in the posterior direction is noticeable, although of smaller magnitude (maximum displacement 0.7 mm). These observations suggest that the deformation described in this mode is rotation of the femur condyles that causes a narrowing of the notch.

Figure 6b shows the 3D displacement of the vertexes related to T3. It is notable that the deformation is not just related to an elevation of the anterior medial plateau (maximum displacement 0.7 mm) that cause the change of the slope, but it involves the other directions as well. The tibia of the ACL patients is shortened in the medial-lateral width and longer in anterior-posterior length. Moreover, a moderate but significant correlation was observed between this 2 modes: p-value = 0.001 Pearson R = 0.38.

Discussion

We developed a novel complex shape analysis method based on 3D MR imaging of the knee and utilized this approach to demonstrate that there are significant shape differences between injured knees and control knees before ACL reconstruction.

Good reproducibility and robustness was found in the first 4 modes of femur and the first 3 of tibia. The shape characteristics that show the largest variability in the examined dataset are represented in earlier modes. These features globally describe the surface, such as size, intercondylar narrowing, and tibia plateau size. Therefore, their characterization is less sensitive to errors in segmentation or in the landmark identification. Moreover, the slice spacing of 1.5 mm can make more difficult the recovery of focus shape features described in the later ranked modes based on differences in patient positioning. Better intra-slice resolution could solve this issue.

In this study a narrowing of notch was observed in the people with ACL injury. This shape characteristic was already outlined in previous studies as a potential risk factor for ACL injury [4]. Using radiographs, Suyral at el.[28] showed that the notch width index (NWI) was significantly smaller in the group that suffered bilateral ACL ruptures when compared with healthy controls and compared with those suffered unilateral ACL ruptures. These results have been reproduced by several other studies most of them using radiographic-based techniques [4, 29, 30]. Nevertheless, some authors have shown no relation between the ACL injury and NWI[31, 32].

In[33] the authors showed that there is no correlation between the x-Ray NWI measure and the overall volume of the notch. Moreover, the results in the estimation of the NWI are strongly affected by the knee flexion angle during the scan.

Compared to previous studies, our approach using SSM and 3D MRI to describe the bone shape is invariant to the knee position with the 3D nature of MR images, and the fully automatic method helps to minimize the operator variability in the measure. Moreover, the 3D modeling can provide a more comprehensive description of the shape changes showing that the shape features that differentiate ACL injured and control subjects is a rotation of the femur condyles that causes a narrowing of the notch. This complex 3D mechanism of notch narrowing cannot be easily described using manually measurable indexes. The potential of SSM is that it provides a measure of this shape feature in an unbiased way. Moderate but significant correlation was observed between T3 and F2.

As previously reported by Mahfouz et al. [34] a significant increase in mode F2 that leads to a smaller intercondylar notch was observed in the female subjects than in male subjects beyond the expected difference in size (1st mode). This may at least partially explain the higher risk of female subjects to sustain an ACL injury as compared to male subjects. [35]

Significant differences were found in the third mode of the tibia between injured and control and between contralateral and control tibias. This mode is related to an elevation of the medial anterior plateau that generates an increase of the posterior tibial slope. Wordeman at. el.[7] recently published a systematic review and meta-analysis on this topic, analyzing fourteen approaches, including studies based on both radiography and MR imaging. The study showed that the majority of the radiographic approaches report tibial plateau slope as a risk factor for ACL injury but just one of the seven MRI studies confirm this result. This review shows that there is vast disagreement regarding the actual values of the slope that would be considered at risk. Our model, however, showed that the bony shape that actually differentiates the ACL injured and control groups is more complex then just an increase of the slope easily detectable in 2D but involves the size of tibiae plateaus in anterio-posterior and medial-lateral directions.

The relevance of this work is in clarifying the relationship between bony anatomy and a higher risk of ligamentous injury. There has been much interest in developing prevention programs to decrease the rate of ACL injuries, and understanding the factors that place certain athletes at a higher risk of sustaining these injuries can help refine these efforts. It is not practical to screen all patients or athletes with cross-sectional imaging, but the

information from this cohort will lead to further investigation of the role in bony shape on ligamentous injuries.

Despite the promising results, there are several limitations of the study. Using 2D FSE images, the present study is limited by a relatively low resolution, especially in the slice direction. A 3D high-resolution image could potentially help with increasing the reliability in the later modes making possible the detection of more focused shape deformation. The sample size is relatively small. The application of the technique on a bigger cohort can substantiate the results obtained in this study. This study is also limited by its cross-sectional nature.

In conclusion, our experiments show that there are significant shape differences between the ACL-injury knees and control knees at baseline. Some of these observed changes in shape align with factors identified in previous studies, but the 3D modeling provides a more comprehensive description of the shape changes in multiple directions. Statistical Shape Modeling with 3D images has the great potential to extract shape features in a completely non–model based approach that looks for the features that actually describe the analyzed surface and avoid a priori choice of relevant indices, like NWI or tibial slope. Bone shape quantification has the great potential to identify specific risk factors for ACL injuries. Such information can help with identifying subjects with an increased risk for suffering an ACL injury and develop targeted prevention strategy including education and training.

Moreover, ACL tears are a well-known risk factor for the development of early post-traumatic osteoarthritis[36,37]. A future application of SSM will be to evaluate the role of the bony shape change for the evaluation of post-traumatic OA risk factors by following up these patients after ACL injury and reconstruction.

Acknowledgments

Role of the Funding Source: This study was supported by NIH/NIAMS P50 AR060752

References

1. Hunter DJ, Lohmander LS, Makovey J, Tamez-Peña J, Totterman S, Schreyer E, et al. The effect of anterior cruciate ligament injury on bone curvature: exploratory analysis in the KANON trial. Osteoarthritis Cartilage. 2014; 22:959–68. [PubMed: 24867633]
2. Myer GD, Ford KR, Hewett TE. New method to identify athletes at high risk of ACL injury using clinic-based measurements and freeware computer analysis. Br J Sports Med. 2011; 45:238–44. [PubMed: 21081640]
3. Myer GD, Ford KR, Khoury J, Succop P, Hewett TE. Clinical correlates to laboratory measures for use in non-contact anterior cruciate ligament injury risk prediction algorithm. Clin Biomech. 2010; 25:693–99.
4. Beynnon BD. Risk factors for anterior cruciate ligament injury: a review of the literature - part 1: neuromuscular and anatomic risk. Sports Health. 2012; 4:69–78. [PubMed: 23016072]
5. Hashemi J, Chandrashekar N, Beynnon BD, Slauterbeck JR, Schutt RC. The geometry of the tibial plateau and its influence on the biomechanics of the tibiofemoral joint. J Bone Joint Surg Am. 2008; 90:2724–34. [PubMed: 19047719]
6. Shao Q, MacLeod TD, Manal K, Buchanan TS. Estimation of Ligament Loading and Anterior Tibial Translation in Healthy and ACL-Deficient Knees During Gait and the Influence of Increasing

Tibial Slope Using EMG-Driven Approach. Ann Biomed Eng. Jan.2011 39:110–121. [PubMed: 20683675]

7. Wordeman SC, Quatman CE, Kaeding CC, Hewett TE. In vivo evidence for tibial plateau slope as a risk factor for anterior cruciate ligament injury: a systematic review and meta-analysis. Am J Sports Med. 2012; 40:1673–81. [PubMed: 22539537]
8. Cootes FT, Taylor CY, Cooper DH, Graham J. Active Shape Models-Their Training and Application Computer Vision and Image Understanding. 1995; 61:38–59.
9. Gregory JS, Waarsing JH, Day J, Pols HA, Reijman M, Weinans H, et al. Early identification of radiographic osteoarthritis of the hip using an ac- tive shape model to quantify changes in bone morphometric features. Arthritis Rheum. 2007; 56:3634–43. [PubMed: 17968890]
10. Lynch JA, Parimi N, Chaganti RK, Nevitt MC, Lane NE. for the Study of Osteoporotic Fractures (SOF) Research Group. The association of proximal femoral shape and incident radiographic hip OA in elderly women. Osteoarthritis and Cartilage. 2009; 17:1313–18. [PubMed: 19427402]
11. Baker-LePain JC, Lynch JA, Parimi N, McCulloch CR, Nevitt MC, Corr M, et al. Variant Alleles of the WNT Antagonist FRZB Are Determinants of Hip Shape and Modify the Relationship between Hip Shape and Osteoarthritis. Arthritis Rheum. 2012; 64(5):1457–1465. [PubMed: 22544526]
12. Haverkamp D, Schiphof, Bierma-Zeinstra SM, Weinans H, Waarsing JH. Variation in Joint Shape of Osteoarthritic Knees. Arthritis Rheum. 2011; 63:3401–07. [PubMed: 21811994]
13. Bredbenner TL 1, Eliason TD, Potter RS, Mason RL, Havill LM, Nicolella DP. Statistical shape modeling describes variation in tibia and femur surface geometry between Control and Incidence groups from the osteoarthritis initiative database. J Biomech. 2010; 43:1780–6. [PubMed: 20227696]
14. Neogi T, Bowes MA, Niu J, De Souza KM, Vincent GR, Goggins J, et al. Magnetic Resonance Imaging–Based Three-Dimensional Bone Shape of the Knee Predicts Onset of Knee Osteoarthritis. Arthritis Rheum. 2013; 68(8):2048–58. [PubMed: 23650083]
15. Rusinkiewicz S, Levoy M. Efficient variants of the ICP algorithm. Proceedings on International Conference on 3-D Digital Imaging and Modeling. 2001:145–52.
16. Sharma, Horaud R, Cech J, Boyer E. Topologically-robust 3D shape matching based on diffusion geometry and seed growing. IEEE Conference on Computer Vision and Pattern Recognition. 2001:2481–88.
17. Hahnel D, Thrun S, Burgard W. An extension of the ICP algorithm for modeling nonrigid objects with mobile robots. Proceedings of the International Joint Conference on Artificial Intelligence. 2003:915–20.
18. Ovsjanikov M, Mérigot Q, Memoli F, Guibas L. One point isometric matching with the heat kernel. Computer Graphics Forum. 2010; 29:1555–64.
19. Sharma, Horaud R, Cech J, Boyer E. Topologically-robust 3D shape matching based on diffusion geometry and seed growing. IEEE Conference on Computer Vision and Pattern Recognition. 2011:2481–88.
20. Davies RY, Twining CY, Cootes TF, Waterton JC, Taylor CY. 3D statistical shape models using direct optimisation of description length. Proc European Conference on Computer Vision, Part III. 2002:3–20.
21. Heimann T, Oguz I, Wolf I, Styner M, Meinzer H. Implementing the automatic generation of 3D statistical shape models with ITK. The Insight Journal—2006 MICCAI Open Science Worksho. 2006
22. Lombaert H, Grady L, Polimeni JR, Cheriet F. FOCUSR: feature oriented correspondence using spectral regularization a method for precise surface matching. IEEE Trans Pattern Anal Mach Intell. 2013; 35:2143–60. [PubMed: 23868776]
23. Carballido-Gamio J, Bauer JS, Stahl R, Lee KY, Krause S, Link TM, et al. Inter-subjec comparison of MRI knee cartilage thickness. Med Image Anal. 2008; 12(2):120–135. [PubMed: 17923429]
24. Lansdown DA, Zaid M, Pedoia V, Subburaj K, Souza R, Ma BC, Li X. Reproducibility measurements of three methods for calculating in vivo MR-based knee kinematics. Journal of Magnetic Resonance Imaging. 2014 in Press.
25. Lorensen, William E.; Cline, Harvey E. Marching Cubes: A high resolution 3D surface construction algorithm. Computer Graphics. 1987:21.

26. Desbrun M, Meyer M, Schröder P, Barr AH. Implicit fairing of irregular meshes using diffusion and curvature flow. Proceedings of the 26th annual conference on Computer graphics and interactive techniques (SIGGRAPH '99). 1999
27. Besl PJ, McKay ND. A Method for Registration of 3-D Shapes. IEEE Trans on Pattern Analysis and Machine Intelligence. 1992; 14:239–56.
28. Souryal TO, Moore HA, Evans JP. Bilaterality in anterior cruciate ligament injuries. Am J Sports Med. 1988; 16:449–54. [PubMed: 3189676]
29. Souryal TO, Freeman TR. Intercondylar notch size and anterior cruciate ligament injuries in athletes. Am J Sports Med. 1993; 21:535–39. [PubMed: 8368414]
30. Dienst D, Schneider G, Altmeyer K, Voelkering K, Georg T, Kramann B, et al. Correlation of intercondylar notch cross sections to the ACL size: a high resolution MR tomographic in vivo analysis. Arch Orthop Trauma Surg. 2007; 127:253–26. [PubMed: 16807752]
31. Stein V, Li L, Guermazi A, Zhang Y, Kwoh KA, Eaton CB, et al. The relation of femoral notch stenosis to ACL tears in persons with knee osteoarthritis. 2010; 18:192–99.
32. Lombardo S, Sethi PM, Starkey C. Intercondylar notch stenosis is not a risk factor for anterior cruciate ligament tears in professional male basketball players: an 11-year prospective study. Am J Sports Med. 2005; 33:29–34. [PubMed: 15610996]
33. val Eck, Carola F.; Martinez, Cesar A Q.; Lorenz, Stephan G F.; Fu, Freddie H.; Smoliski, P. Assessment of correlation between knee notch width index and the three-dimensional notch volume. Knee Surg Sports Traumatol Arthrosc. 2010; 18:1239–44. [PubMed: 20376620]
34. Mahfouz M, Abdel Fatah EE, Bowers LS, Scuderi G. Three-dimensional Morphology of the Knee Reveals Ethnic Differences. Clinical Orthopaedics and Related Research. 2012; 470(1):172–185. [PubMed: 21948324]
35. Smith HC, Vacek P, Johnson RJ, Slauterbeck J, Hashemi R, Shultz J, et al. Risk Factors for Anterior Cruciate Ligament Injury: A Review of the Literature—Part 2: Hormonal, Genetic, Cognitive Function, Previous Injury, and Extrinsic Risk Factors.
36. Lohmander LS, Ostenberg A, Englund M, Roos H. High prevalence of knee osteoarthritis, pain, and functional limitations in female soccer players twelve years after anterior cruciate ligament injury. Arthritis Rheum. 2004; 50:3145–52. [PubMed: 15476248]
37. Von Porat A, Roos EM, Roos H. High prevalence of osteoarthritis 14 years after an anterior cruciate ligament tear in male soccer players: a study of radiographic and patient relevant outcomes. Ann Rheum Dis. 2004; 63:269–73. [PubMed: 14962961]

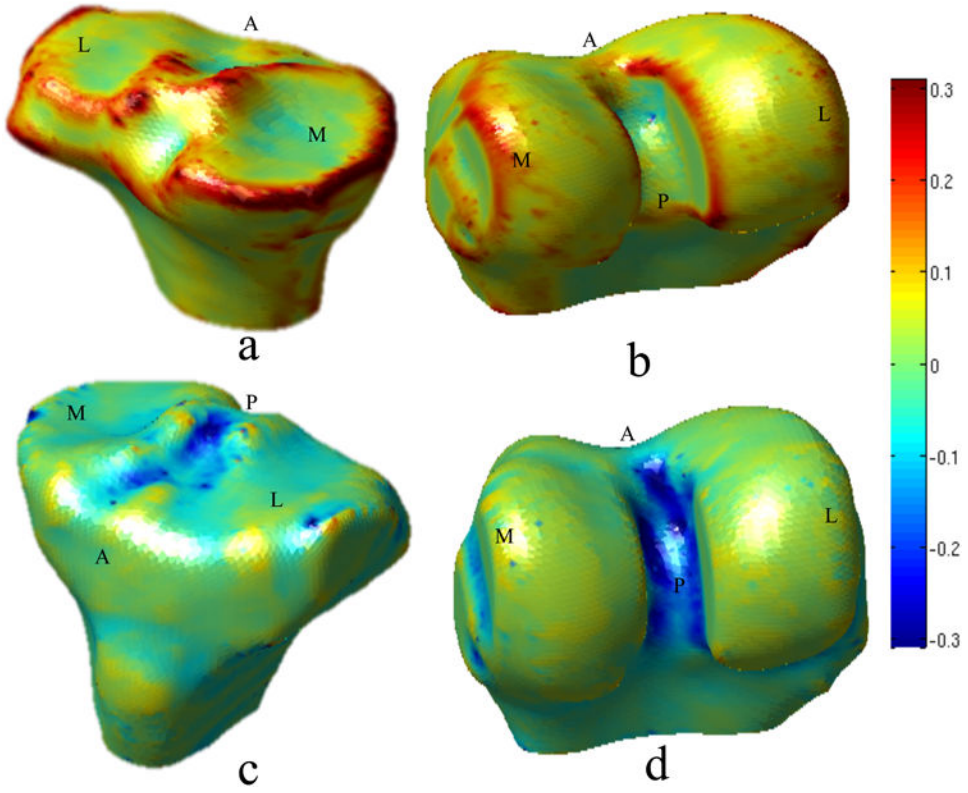

Figure 1.

Spatial distribution of the principal curvatures on the reference surfaces of tibia and femur. a) Tibia maximum curvature k1. b) Femur maximum curvature k1. c) Tibia minimum curvature k2. d) Femur minimum curvature k2. Directions are labeled in the figure. M: medial, L: lateral, A: anterior P: posterior

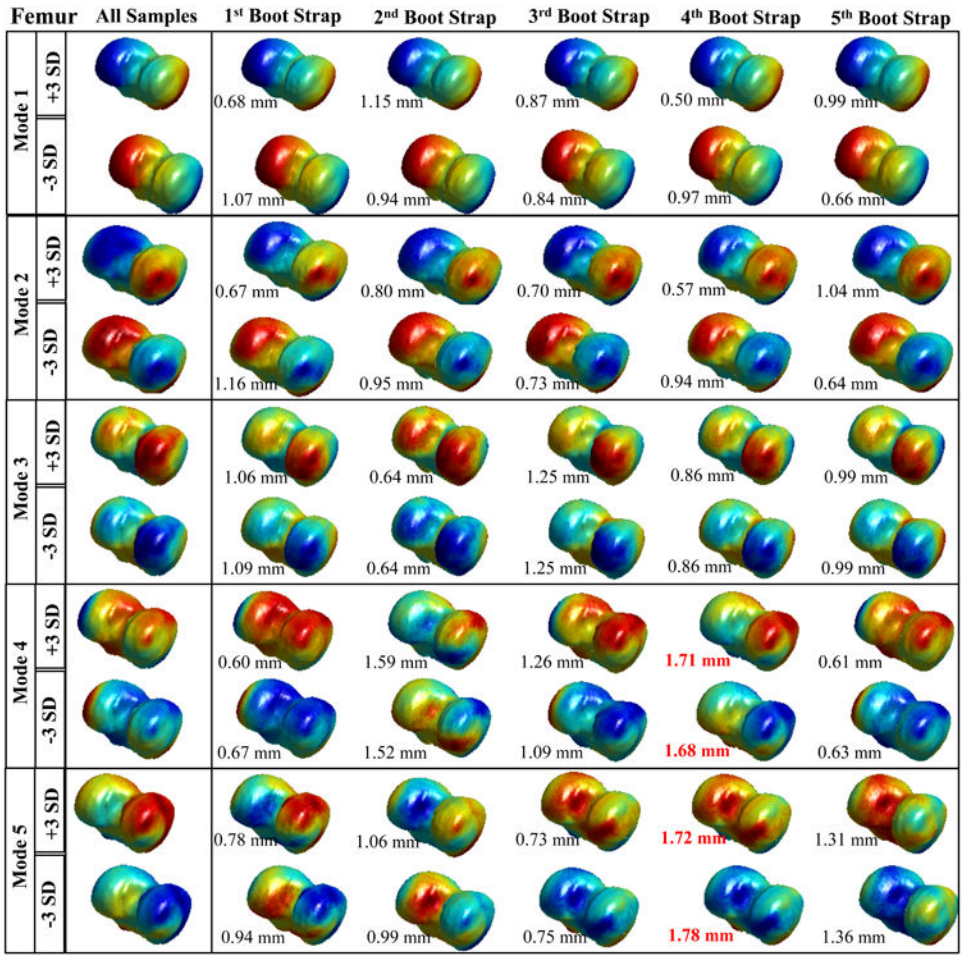

Figure 2.

Results of the Femur bootstrapping experiment. Spatial distribution of the vertex displacements assigned to mode values equal to: mean +3*standard deviation and mean – standard deviation. Each row represents a different modes form 1 to 5. The first column shows the model obtained with the whole cohort (119 knees). The rows 2-6 show the spatial distribution of the displacement for the different bootstrap together with the average distance between the fully sampled model.

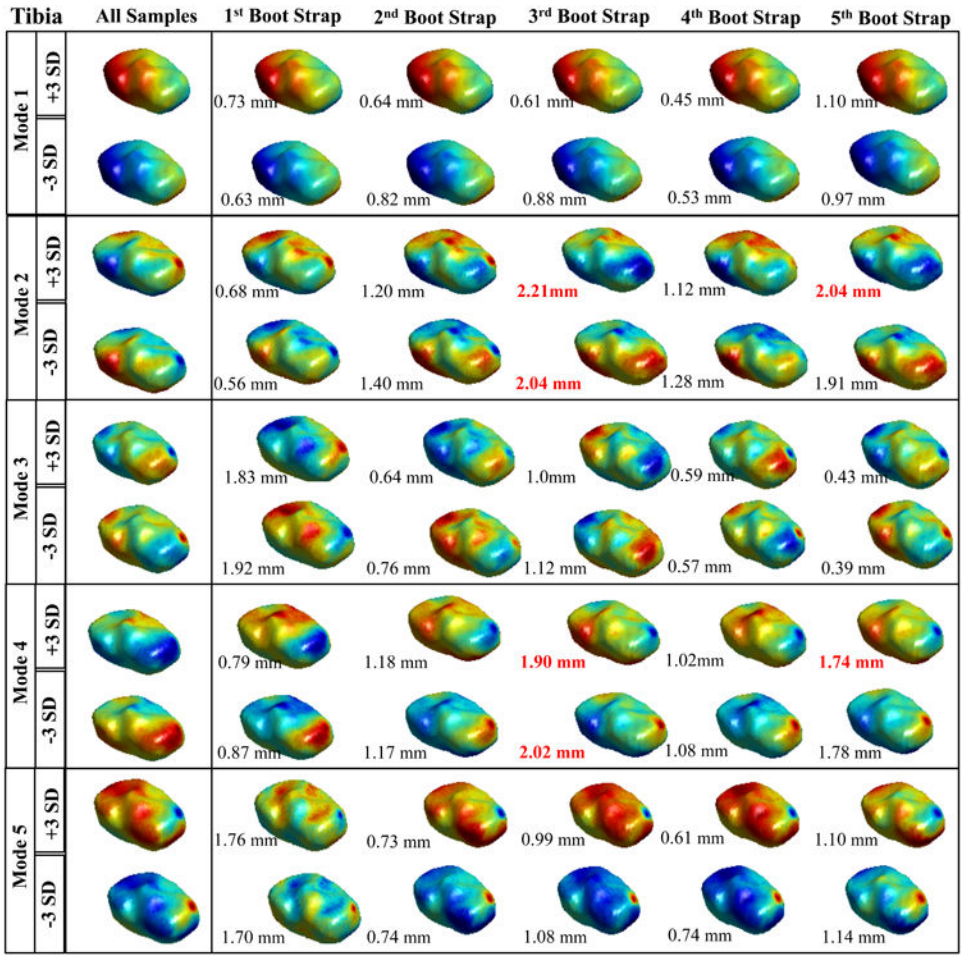

Figure 3.

Results of the Tibia bootstrapping experiment. Spatial distribution of the vertex displacements assigned to mode values equal to: mean +3*standard deviation and mean – standard deviation. Each row represents a different modes form 1 to 5. The first column shows the model obtained with the whole cohort (119 knees). The rows 2-6 show the spatial distribution of the displacement for the different bootstrap together with the average distance between the fully sampled model.

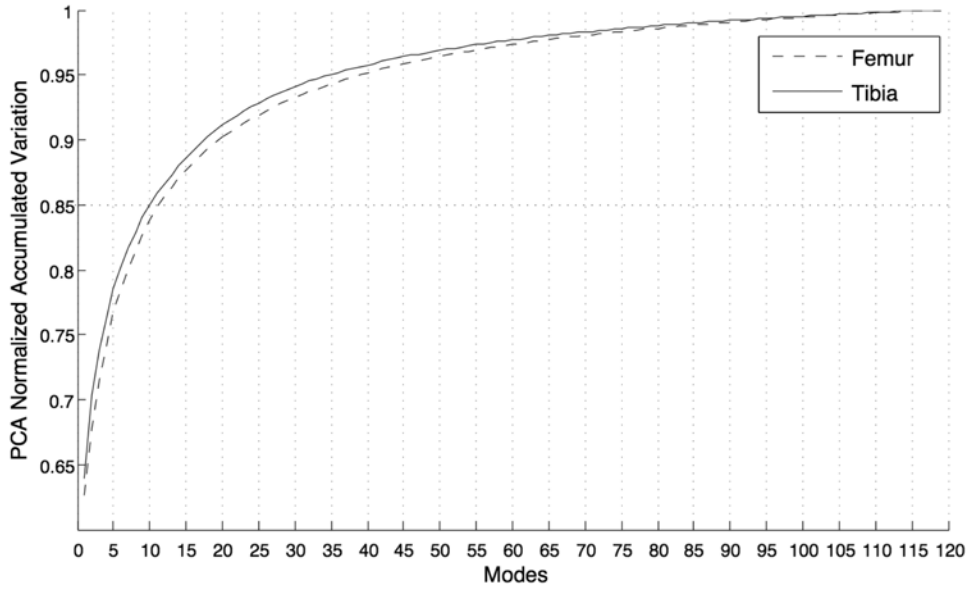

Figure 4.

Representation of the model's compactness: cumulative % of the variability expressed in function of the number of modes considered in the model.

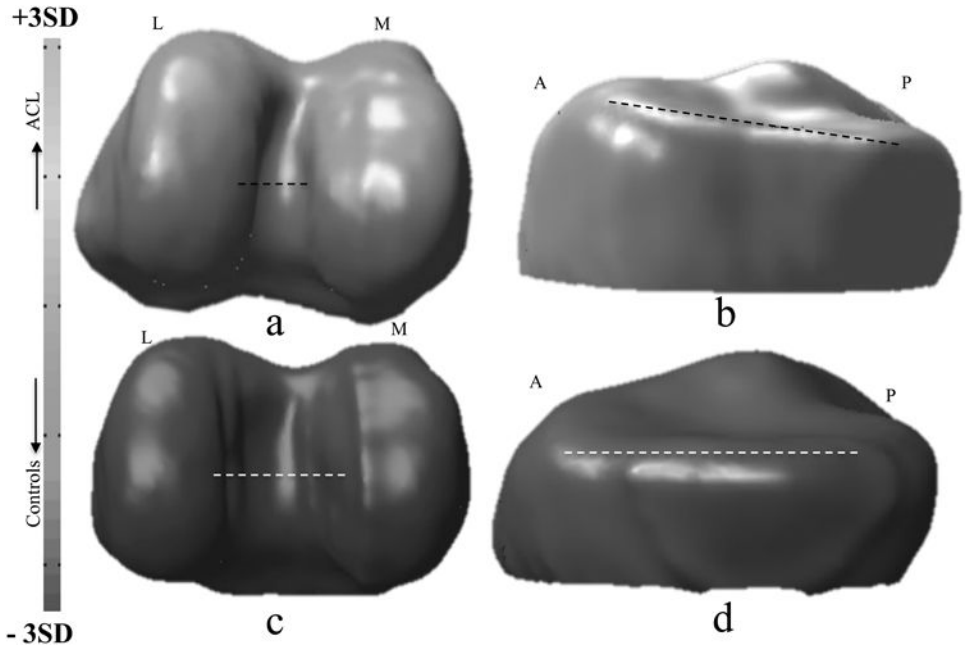

Figure 5.

modeling of the principal component F2 (a,c) and T3 (b,d) of the scale-preserved model. In the first row Mean + 3STD. in the second row Mean − 3STD. Directions are labeled in the figure. M: medial, L: lateral, A: anterior P: posterior

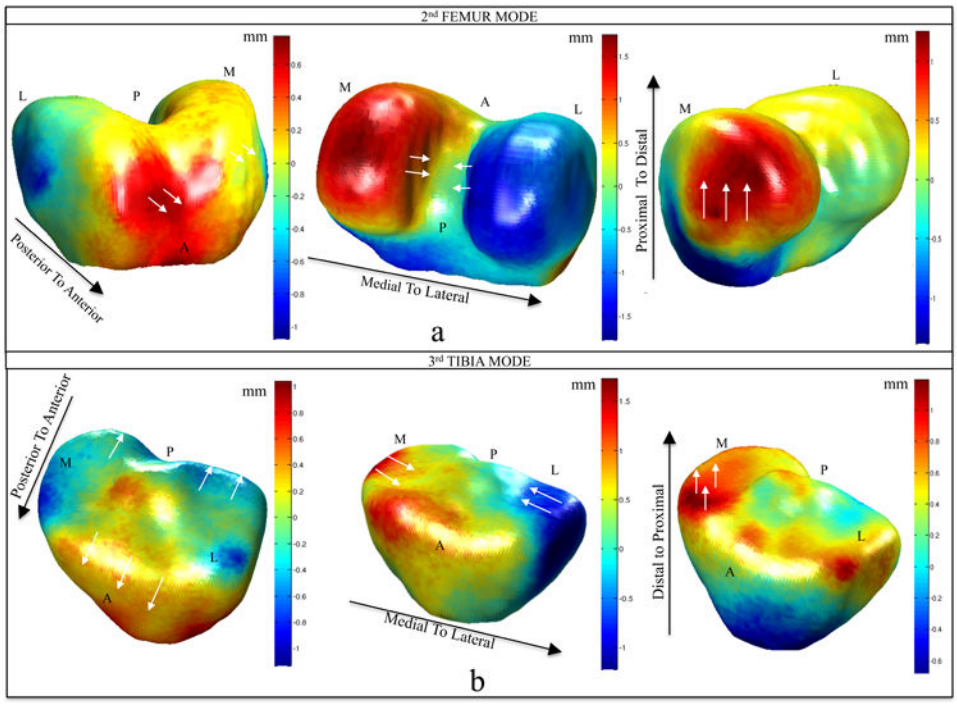

Figure 6.

Displacement of the vertices modeling the difference between injured and control knees in the modes F2 (a), T3 (b) of the scale-preserved model. The black arrows show the direction of the displacement represented in each mesh. Posterior to anterior: positive values (red) displacement towards anterior direction, negative values (blue) displacement towards posterior direction. Medial to lateral: positive values (red) displacement towards lateral direction, negative values (blue) displacement towards medial direction. Distal to proximal: positive values (red) displacement towards proximal direction, negative values (blue) displacement towards distal direction. The white arrows show locally on the mesh the directions of the vertexes displacement. Directions are labeled in the figure. M: medial, L: lateral, A: anterior P: posterior

Table 1

Inter-User and Scan-Rescan reliability: RMS- CV computed for the first 10 modes on 3 subjects after two post processing section performed by 2 users reliability: Coefficients of Variations (CV) computed for the first 10 modes on 5 subjects scanned and processed twice after repositioning.

	Mode 1	Mode 2	Mode 3	Mode 4	Mode 5	Mode 6	Mode 7	Mode 8	Mode 9	Mode 10
Inter - User RMS-CV (%)										
Femur	2.27	1.60	3.42	0.98	4.99	11.35	6.77	13.19	16.64	11.09
Tibia	0.71	4.12	1.46	7.36	10.68	3.68	8.02	7.49	12.51	16.70
Scan - Rescan RMS-CV (%)										
Femur	1.66	7.14	7.34	7.78	12.73	18.31	9.25	27.16	10.89	20.26
Tibia	2.65	7.08	8.35	20.10	22.46	19.68	14.89	20.27	13.17	18.38

Table 2

Results obtained analyzing the difference between: injured and control knees shape; contralateral and control knees shape and injured and contralateral knees. Significance p-value <0.01. (a,b) Surfaces rigidly aligned (c,d) Surfaces Euclidean aligned.

(a)	
2nd Mode Femur (scale-preserved dataset)	
ACL injured	365.55 (84.41)
Control	306.89 (60.89)
P-value (unpaired Ttest)	***0.007**
Contralateral	351.65 (81.58)
Control	306.89 (60.89)
P-value (unpaired Ttest)	0.03
ACL injured	365.55 (84.41)
Contralateral	351.65 (81.58)
P-value (paired Ttest)	0.03

(b)	
3rd Mode Tibia (scale-preserved dataset)	
ACL injured	107.06 (40.06)
Control	70.47 (47.21)
P-value (unpaired Ttest)	***0.002**
Contralateral	111.59 (44.45)
Control	70.47 (47.21)
P-value (unpaired Ttest)	***0.001**
ACL injured	107.06 (40.06)
Control	111.59 (44.45)
P-value (paired Ttest)	0.32

(c)	
1st Mode Femur (Euclidean aligned dataset)	
ACL injured	292.85 (88.26)
Control	231.72 (65.11)
P-value (unpaired Ttest)	***0.007**
Contralateral	281.69 (82.96)
Control	231.72 (65.11)
P-value (unpaired Ttest)	0.021
ACL injured	292.85 (88.26)
Contralateral	281.69 (82.96)
P-value (paired Ttest)	0.11

(d)	
2nd Mode Tibia (Euclidean aligned dataset)	
ACL injured	79.52 (23.17)
Control	61.00 (24.51)
P-value (unpaired Ttest)	***0.004**
Contralateral	84.9 (35.38)
Control	61.00 (24.51)
P-value (unpaired Ttest)	***0.009**
ACL injured	79.52 (23.17)
Control	61.00 (24.51)
P-value (paired Ttest)	0.34